Journal of Solid State Chemistry **161,** 225–232 (2001)
doi:10.1006/jssc.2001.9303, available online at http://www.idealibrary.com on IDEAL®

$KLnTiO_4$ (Ln = La, Nd, Sm, Eu, Gd, Dy): A New Series of Ruddlesden–Popper Phases Synthesized by Ion-Exchange of $HLnTiO_4$

Raymond E. Schaak and Thomas E. Mallouk[1]

Department of Chemistry, The Pennsylvania State University, University Park, Pennsylvania 16802-6300, USA

Received March 27, 2001; in revised form June 19, 2001; accepted July 12, 2001

$KLnTiO_4$ (Ln = La, Nd, Sm, Eu, Gd, Dy), a new series of $n = 1$ Ruddlesden–Popper phases, was synthesized by a two-step ion-exchange reaction. $HLnTiO_4$ was first prepared by traditional acid exchange of $NaLnTiO_4$, and the $KLnTiO_4$ series was subsequently formed from the reaction of $HLnTiO_4$ with hot aqueous KOH. The ion exchange is stoichiometric, and the $KLnTiO_4$ phases are thermally stable to at least 700°C. All the $KLnTiO_4$ phases are orthorhombic and crystallize in space group *Pbcm*. The structures of $KSmTiO_4$, $KEuTiO_4$, $KGdTiO_4$, and $KDyTiO_4$ were refined by the Rietveld method and found to be isostructural with their $NaLnTiO_4$ precursors. All the $KLnTiO_4$ phases form stable hydrates when exposed to a humidified atomosphere. © 2001 Academic Press

INTRODUCTION

Transition-metal oxides that adopt the perovskite structure (1) possess a wide variety of interesting properties, including superconductivity (2), colossal magnetoresistance (3), ferroelectricity (4), and catalytic activity (5), depending on the choice and stoichiometry of the A- and B-site cations. Layered perovskites that belong to the Ruddlesden–Popper (6) $A_2[A'_{n-1}B_2O_{3n+1}]$ (A = alkali, A' = alkaline earth or rare earth, and B = transition metal), and Dion–Jacobson (7), $A[A'_{n-1}B_2O_{3n+1}]$, families possess similar properties. For example, the Ruddlesden–Popper manganate family $(La,Sr)_{n+1}Mn_nO_{3n+1}$ exhibits colossal magnetoresistance (3), and spontaneously hydrated layered perovskites such as $K_2La_2Ti_3O_{10}$ catalyze the photolytic decomposition of water (5a).

Layered perovskites can be described structurally as two-dimensional perovskite slabs that are separated by ion-exchangeable interlayer cations, which makes them especially intriguing as precursors to new low-temperature and metastable perovskite phases. In recent years, several new topochemical solid-state reactions have been reported, and it is now possible to design new perovskites in a rational, stepwise process to target interesting and otherwise inaccessible structural features. By applying a predetermined sequence of textbook-style reactions, one can synthesize perovskites that have controlled A-site vacancies (8), ordered A-site cations in nondefective phases (9), and perovskite intergrowths with a variety of two-dimensional structural units (10).

The topochemical transformations that convert layered perovskites into new layered and three-dimensional phases rely on the facile ion exchange of the monovalent interlayer cations, which can be replaced with divalent or smaller monovalent cations in simple aqueous (9, 11), molten-salt (9, 12, 13), and solid–solid (14, 15) ion-exchange reactions. In general, it is difficult to replace an interlayer cation with a larger cation of the same charge since a higher charge density is usually needed to drive the ion-exchange reaction. This is a severe limitation when designing new phases since the structures and properties of a material can change dramatically as the size of the interlayer cation changes. Ruddlesden–Popper phases for example, rarely form stable hydrates when a small alkali cation such as Na^+ or Li^+ occupies the interlayer space, but readily hydrate when the interlayer gallery is expanded by a larger cation such as K^+ (16). Interestingly, the photocatalytic properties of layered perovskites that split H_2O into H_2 and O_2 are also positively correlated with the ability of the layered perovskite to form a stable hydrate (5a). Thus, the most efficient Ruddlesden–Popper photocatalysts have K^+ (or Rb^+) between the perovskite layers.

In the rational search for new materials, the ability to replace an interlayer cation with a larger cation of the same charge would be a useful tool for studying the structure–property relationships in a series of compounds that have subtle structural differences. The $n = 1$ Ruddlesden–Popper phase $NaLnTiO_4$ (Ln = lanthanide) is an interesting target for low-temperature modification since its

[1]To whom correspondence should be addressed.

0022-4596/01 $35.00

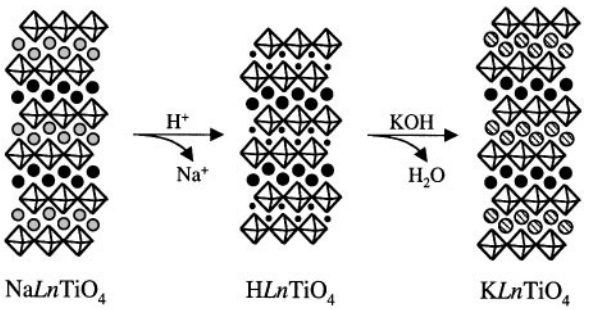

FIG. 1. Two-step ion-exchange reaction for synthesizing $KLnTiO_4$. Large black circles represent *Ln*, gray circles represent Na, small black circles represent H, hatched circles represent K, and the octahedra represent TiO_6 units.

unique structure facilitates its conversion into a variety of layered phases. $NaLnTiO_4$ consists of single layers of TiO_6 octahedra that are separated in alternate layers by Na^+, which is ion-exchangeable, and Ln^{3+}, which is not exchangeable (Fig. 1a) (17). The ordering of the Na^+ and Ln^{3+} cations depends crucially on both their charge difference and their similar size, so phases such as $LiLnTiO_4$ and $KLnTiO_4$ cannot be synthesized at high temperatures. However, molten-salt exchange of Na^+ for Li^+ has been used to synthesize $LiLnTiO_4$, which exhibits lithium ion conductivity (13), and $HLnTiO_4$ is formed by proton exchange in dilute acid (18). $HLnTiO_4$ topochemically dehydrates to form the A-site defective $n = 2$ Ruddlesden–Popper phase $Ln_2\square Ti_2O_7$ (19), which transforms to the ferroelectric phase $Ln_2Ti_2O_7$ at higher temperatures. $Ca_{0.5}EuTiO_4$, formed by divalent ion exchange of $NaEuTiO_4$, topochemically reduces to form the nondefective $n = 2$ phase $Eu_2CaTi_2O_7$ (11). In addition, divalent ion exchange of $NaLaTiO_4$ with Ca^{2+}, along with reductive intercalation of Na^0, can be used to carefully control the mixed valency of Ti in $Na_{1-x}Ca_{x/2}LaTiO_4$ (15).

In this paper, we present a two-step approach for synthesizing the potassium form of $ALnTiO_4$ (A = alkali), which is an important addition to the family of structurally similar $n = 1$ Ruddlesden–Popper phases. First, the proton form of $NaLnTiO_4$ is accessed by traditional acid exchange. The series $KLnTiO_4$ (*Ln* = La, Nd, Sm, Eu, Gd, Dy) is then formed from the reaction of $HLnTiO_4$ with KOH, which shifts the driving force of the ion-exchange reaction from charge density and mass action to acid/base chemistry. The $KLnTiO_4$ phases readily hydrate, and this could have interesting implications for their utility in the photocatalytic decomposition of water.

EXPERIMENTAL

$NaLnTiO_4$ was prepared as previously reported (17), by heating stoichiometric mixtures of Na_2CO_3, Ln_2O_3, and TiO_2 for 30 min at 950°C (*Ln* = La, Sm, Eu, Gd, Dy) or 900°C (*Ln* = Nd). Ln_2O_3 was heated to 900°C for several hours prior to use to remove water and carbonate impurities, and a 40% excess of Na_2CO_3 was used to compensate for loss due to volatilization. $HLnTiO_4$ was formed by acid exchange in 0.1 M HNO_3 for 1 day. $KLnTiO_4$ was synthesized by stirring 1 g of $HLnTiO_4$ in 100 mL of 1 M KOH for 3 days at 60°C. The $KLnTiO_4$ phases were dried at 500°C for 12 h prior to analysis. Hydrated $KLnTiO_4 \cdot xH_2O$ phases were obtained by exposing the powders to a humidified atmosphere for 3 days.

X-ray diffraction (XRD) patterns were obtained on a Philips X-Pert MPD diffractometer in θ–θ geometry using monochromatized Cu$K\alpha$ ($\lambda = 1.5418$ Å) radiation. Profile fitting and refinement of the lattice parameters and atomic positions were performed by the Rietveld method (20) using the GSAS structure refinement package (21). Energy-dispersive *X*-ray emission analysis (EDAX) was performed on a JEOL-JSM 5400 scanning electron microscope at 30-kV accelerating voltage. EDAX data was obtained at the Electron Microscope Facility for the Life Sciences in the Biotechnology Institute at the Pennsylvania State University. Data from at least four acquisitions were averaged to obtain the reported results.

RESULTS AND DISCUSSION

Synthesis and the Acid/Base Ion-Exchange Reaction

$KLnTiO_4$ was synthesized by the two-step ion-exchange reaction depicted in Fig. 1. The alkali precursors, $NaLnTiO_4$, were synthesized according to literature methods (17), and their X-ray diffraction patterns and lattice parameters matched those reported previously. The XRD data for the $HLnTiO_4$ phases also agreed with literature values (18) and EDAX confirmed the removal of all the sodium during the acid exchange. Upon reaction in hot aqueous KOH for several days, $HLnTiO_4$ was stoichiometrically converted to $KLnTiO_4$. The EDAX data presented in Table 1 confirm that all the protons were replaced by K^+, within experimental error, indicating that the acid/base

TABLE 1
EDAX Data for $KLnTiO_4$

Compound	Elemental ratios[a]		
	K	Ln	Ti
$KLaTiO_4$	1.00	1.07	1.00
$KNdTiO_4$	1.05	0.95	1.00
$KSmTiO_4$	0.96	0.97	1.00
$KEuTiO_4$	0.94	0.98	1.00
$KGdTiO_4$	0.95	0.99	1.00
$KDyTiO_4$	1.08	0.98	1.00

[a] Atomic ratios normalized to Ti.

reaction goes to completion. This is in contrast to many other molten salt, aqueous, and solid–solid ion exchanges in layered perovskites, which often exchange only 70–90% of their interlayer cations. Apparently, the acid/base neutralization reaction not only facilitates ion exchange of a larger cation, but it also provides a route to a higher efficiency ion exchange.

All the K*Ln*TiO$_4$ phases are thermally stable up to 700°C, where they begin to decompose to other layered perovskite or pyrochlore phases. This is in contrast to the Na*Ln*TiO$_4$ phases, which are stable beyond 950°C, and the H*Ln*TiO$_4$ phases, which dehydrate to $Ln_2\square Ti_2O_7$ around 500°C and transform to $Ln_2Ti_2O_7$ (110)-layer perovskite (*Ln* = La) or pyrochlore phases upon further heating. The K*Ln*TiO$_4$ phases of the larger lanthanides (*Ln* = La, Nd, Sm, Eu) decompose above 800°C, primarily to the $n = 3$ Ruddlesden–Popper phase $K_2Ln_2Ti_3O_{10}$, although several other phases are present in smaller amounts. KGdTiO$_4$ decomposes partially to $K_2Gd_2Ti_3O_{10}$ around 950°C, and pyrochlore-type $Gd_2Ti_2O_7$ begins forming by 1050°C. KDyTiO$_4$ begins decomposing at 800°C, transforming completely to pyrochlore-type $Dy_2Ti_2O_7$ by 1050°C.

In similar work with other Ruddlesden–Popper phases, we discovered that the acid/base ion-exchange reaction can be generalized to prepare a variety of new phases. For example, $H_2Eu_2Ti_3O_{10}$ (synthesized by proton exchange of $K_2Eu_2Ti_3O_{10}$) can form $A_2Eu_2Ti_3O_{10}$ (*A* = Na, Li) by reaction in hot aqueous *A*OH for several days. In addition, $Na_2Sr_2Nb_2MnO_{10}$, a $n = 3$ Ruddlesden–Popper phase with ordered B-site Nb^{5+} and Mn^{4+} cations, forms from the reaction of $H_2Sr_2Nb_2MnO_{10}$ with hot aqueous NaOH (22). NaEuTiO$_4$, which is structurally identical to the parent phase prepared at 950°C, forms from the aqueous reaction of HEuTiO$_4$ with NaOH. In all cases, the ion exchange is nearly stoichiometric.

In contrast, Jacobson and co-workers reported that the Dion–Jacobson phase $HCa_2Nb_3O_{10}$ reacts with *A*OH (*A* = alkali) to form $H_{1-x}A_xCa_2Nb_3O_{10}$, and the degree of exchange depends on the size of the exchanging cation (23). Accordingly, the equilibrium phases are $Na_{0.77}H_{0.33}Ca_2Nb_3O_{10}$, $K_{0.5}H_{0.5}Ca_2Nb_3O_{10}$, and $Rb_{0.42}H_{0.58}Ca_2Nb_3O_{10}$ for ion exchange with Na^+, K^+, and Rb^+, respectively. Unlike the Ruddlesden–Popper phases, complete exchange of H^+ for A^+ does not occur for the Dion–Jacobson phases (although a higher degree of exchange is possible upon preintercalation of an alkylamine, which expands the interlayer gallery (23)). As in the Dion–Jacobson series, the acid/base reaction can also be controlled in the Ruddlesden–Popper phases to form solid solutions such as $Na_xH_{2-x}Ln_2Ti_3O_{10}$ ($x = 0$ to 2) (24). The degree of exchange depends on both the reaction time and the concentration of *A*OH, but not on the size of the exchanging cation as in the Dion–Jacobson case. In this report, the K*Ln*TiO$_4$ series was reacted to the point of complete exchange to study the structures of these new stoichiometric Ruddlesden–Popper phases.

Structure of KLnTiO$_4$

The XRD patterns for representative K*Ln*TiO$_4$ phases are shown in Fig. 2, and the lattice parameters determined by least-squares refinement of the powder diffraction data are presented in Table 2. All the phases index to an orthorhombic unit cell that is structurally analogous to Na*Ln*TiO$_4$ (*Ln* = Sm, Eu, Gd, Dy) (17), but the layer spacings are significantly larger as expected for the larger K^+ cation. KEuTiO$_4$ and KDyTiO$_4$, shown in Fig. 2, as well as KGdTiO$_4$ and KNdTiO$_4$ are highly crystalline phases that are characterized by sharp diffraction peaks, which can all be indexed to an orthorhombic pattern. KSmTiO$_4$ and KLaTiO$_4$ (as well as most of the hydrated phases that are discussed later), on the other hand, have slightly more peak broadening. Scanning electron microscopy (SEM) images

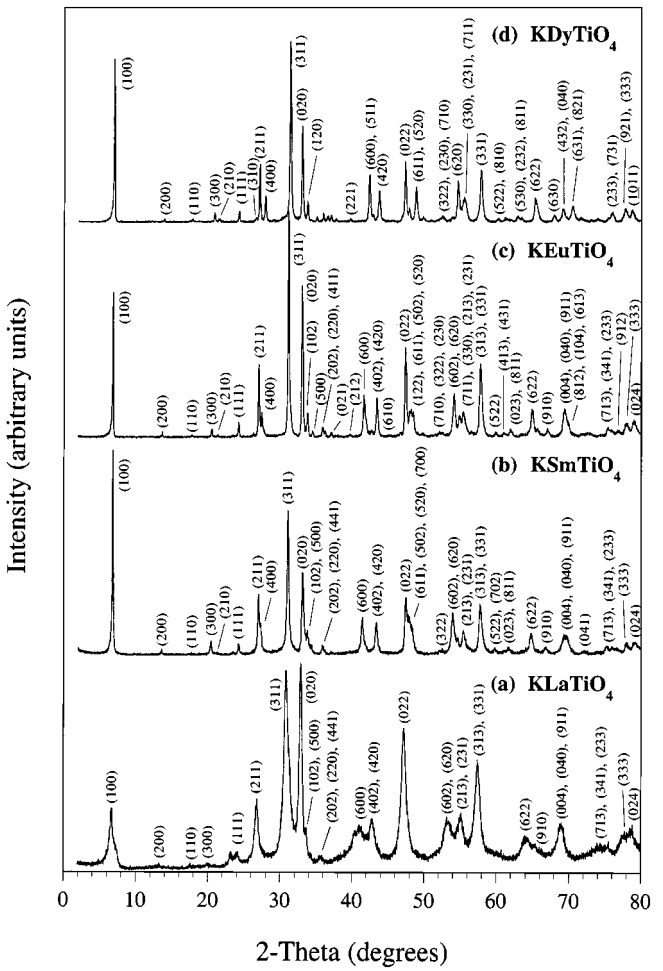

FIG. 2. XRD patterns for (a) KLaTiO$_4$, (b) KSmTiO$_4$, (c) KEuTiO$_4$, and (d) KDyTiO$_4$.

TABLE 2
Lattice Parameter Data for K*Ln*TiO$_4$

Compound	*a* (Å)	*b* (Å)	*c* (Å)	Unit cell volume (Å^3)
KLaTiO$_4$	13.238(3)	5.438(2)	5.466(2)	393.5
KNdTiO$_4$	13.1995(9)	5.4030(6)	5.4166(4)	386.30
KSmTiO$_4$	13.0982(7)	5.4115(5)	5.4242(7)	384.47
KEuTiO$_4$	13.0045(5)	5.4116(4)	5.4205(3)	381.47
KGdTiO$_4$	12.9564(6)	5.4170(6)	5.4228(8)	380.60
KDyTiO$_4$	12.8102(4)	5.4303(5)	5.4299(7)	377.72

Note. Standard deviations are given in parentheses.

indicate that all the K*Ln*TiO$_4$ phases have well-formed crystallites that range in size from 500 nm to 5 μm, and they retain the platelet morphology of their Na*Ln*TiO$_4$ precursors. Thus, the peak broadening for KSmTiO$_4$, KLaTiO$_4$, and the K*Ln*TiO$_4$·xH$_2$O hydrates must arise from structural disorder, most likely along the alkali interlayer.

The structures of K*Ln*TiO$_4$ (*Ln* = Sm, Eu, Gd, Dy) were refined using GSAS, and two representative refinements are shown in Fig. 3. The fractional coordinates and other crystallographic data are presented in Table 3. All the refinements converged reasonably well in the orthorhombic space group *Pbcm*, which confirms that the K*Ln*TiO$_4$ phases are $n = 1$ members of the Ruddlesden–Popper family of layered perovskites and are isostructural with Na*Ln*TiO$_4$ (*Ln* = Sm, Eu, Gd, Dy). There were no stray peaks in the diffraction patterns, which indicates that the samples were nearly phase pure. The structure of KNdTiO$_4$ was not refined due to the presence of multiple hydrated phases, which formed immediately upon removal from the drying oven and were unavoidable during XRD analysis. The structure of KLaTiO$_4$ was also not refined because of extremely broad peaks (Fig. 1a). The X-ray diffraction patterns of KNdTiO$_4$ and KLaTiO$_4$ are similar to those of the other lanthanides, which indicates that the entire K*Ln*TiO$_4$ series is isostructural.

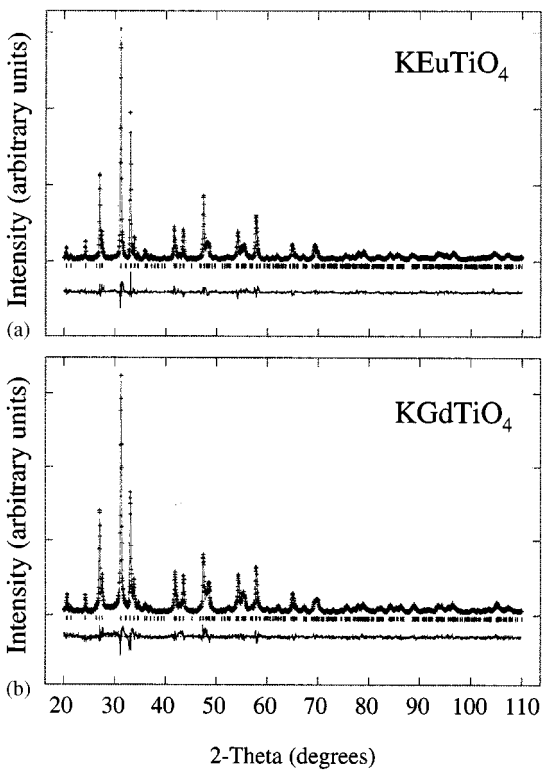

FIG. 3. Rietveld structure refinements for (a) KEuTiO$_4$ and (b) KGdTiO$_4$, showing the calculated (top, solid line) and observed (top, crosses) XRD patterns. The difference curves (bottom, solid line) indicate the agreement between the observed and calculated patterns. Allowed Bragg reflections are indicated below the peaks.

The site occupancies for the K*Ln*TiO$_4$ phases presented in Table 3 refined as expected, with slight deviations from ideal stoichiometry that are within experimental error. The atomic positions did not vary significantly from the starting models, which were based on the analogous Na*Ln*TiO$_4$ compounds (17). The refined thermal parameters are also reasonable, with the largest values for the O(4) atom, which is along the alkali interlayer gallery (see Fig. 4b) and is typically more prone to thermal variation than the other perovskite-block or lanthanide-layer oxygen atoms in similar layered perovskites.

Figure 4 shows two crystallographic views of the refined structure of KEuTiO$_4$, which is also representative of the other lanthanides. Figure 4a shows the unit cell of KEuTiO$_4$ in the *Pbcm* space group, with the **a** axis defined as the stacking axis. The tilting of the TiO$_6$ octahedra is clearly evident, as is the distortion of the Ti^{4+} cation away from the center of the symmetric octahedron and toward the ion-exchangeable interlayer gallery. As in other layered perovskites (8e, 25), electrostatic repulsion between Ln^{3+} and Ti^{4+} forces the Ti^{4+} away from the lanthanide layer and toward the less positively charged K$^+$ layer. The expanded view along the (011) plane of KEuTiO$_4$ in Fig. 4b shows the usual polyhedral view of a Ruddlesden–Popper phase. The cooperative distortions and buckling of the TiO$_6$ octahedra are evident in Fig. 4b, which shows how the tilting of the octahedra alternates from left to right along the (011) plane. It is also evident that the terminal oxygen atoms of the TiO$_6$ octahedra shift closer to the Ln^{3+} cations, which decreases the O(3)–Ti–O(1) bond angle. The shift of the O(4) atom toward the potassium in the alkali layer is much less pronounced due to the lower electrostatic attraction between the oxide anion and the monovalent alkali cation.

Figure 5 shows the lattice parameter trends for the K*Ln*TiO$_4$ series. As expected, the **a** lattice parameter, which is the stacking axis of the layers in the unit cell, decreases nearly monotonically as the size of the lanthanide cation decreases. KLaTiO$_4$ has larger in-plane **b** and **c** lattice

TABLE 3
Crystallographic Data for $KLnTiO_4$ (Ln = Sm, Eu, Gd, Dy)

Compound	Atom	Site occupancy	x	y	z	100 U_{iso} (Å^2)	Wyckoff symmetry
$KSmTiO_4$	K	0.95(1)	0.5901(4)	0.005(2)	0.25	1.0(1)	4*d*
$a = 13.0982(7)$	Sm	0.982(6)	0.8949(1)	0.0120(7)	0.25	1.21(5)	4*d*
$b = 5.4115(5)$	Ti	1.012(8)	0.2507(4)	0.012(2)	0.25	0.9(1)	4*d*
$c = 5.4242(7)$	O(1)	1.04(4)	0.204(1)	0.25	0	1.8(7)	4*c*
$R_f^2 = 9.59\%$	O(2)	1.03(4)	0.764(1)	0.25	0	4.1(9)	4*c*
$R_{wp} = 16.41\%$	O(3)	1.03(2)	0.069(1)	−0.051(3)	0.25	0.1(2)	4*d*
$R_p = 12.75\%$	O(4)	0.99(2)	0.392(1)	0.034(6)	0.25	3.0(7)	4*d*
$KEuTiO_4$	K	1.034(8)	0.5941(3)	0.019(1)	0.25	0.4(1)	4*d*
$a = 13.0045(5)$	Eu	0.960(5)	0.8962(1)	0.0209(4)	0.25	0.90(5)	4*d*
$b = 5.4116(4)$	Ti	1.016(7)	0.2481(3)	0.011(1)	0.25	0.2(1)	4*d*
$c = 5.4205(3)$	O(1)	0.95(3)	0.200(1)	0.25	0	2.3(7)	4*c*
$R_f^2 = 10.86\%$	O(2)	1.05(3)	0.770(1)	0.25	0	0.6(4)	4*c*
$R_{wp} = 14.92\%$	O(3)	1.06(2)	0.0632(9)	−0.064(2)	0.25	0.1(2)	4*d*
$R_p = 11.16\%$	O(4)	1.04(2)	0.381(1)	0.021(4)	0.25	3.7(5)	4*d*
$KGdTiO_4$	K	0.948(9)	0.5935(5)	0.016(2)	0.25	0.9(2)	4*d*
$a = 12.9564(6)$	Gd	1.001(6)	0.8955(1)	0.0186(5)	0.25	0.84(5)	4*d*
$b = 5.4170(6)$	Ti	1.007(8)	0.2495(4)	0.009(1)	0.25	0.8(1)	4*d*
$c = 5.4228(8)$	O(1)	1.04(3)	0.200(1)	0.25	0	0.1(5)	4*c*
$R_f^2 = 9.48\%$	O(2)	1.05(3)	0.770(1)	0.25	0	0.7(5)	4*c*
$R_{wp} = 14.68\%$	O(3)	1.04(2)	0.066(1)	−0.048(3)	0.25	0.1(2)	4*d*
$R_p = 10.95\%$	O(4)	0.97(2)	0.379(1)	0.050(5)	0.25	5.3(8)	4*d*
$KDyTiO_4$	K	0.996(8)	0.5946(3)	0.019(1)	0.25	0.4(1)	4*d*
$a = 12.8102(4)$	Dy	0.983(5)	0.8965(1)	0.0254(3)	0.25	0.81(4)	4*d*
$b = 5.4303(5)$	Ti	1.013(7)	0.2483(3)	0.012(1)	0.25	0.2(1)	4*d*
$c = 5.4299(7)$	O(1)	1.04(2)	0.198(1)	0.25	0	0.1(2)	4*c*
$R_f^2 = 9.97\%$	O(2)	1.05(3)	0.772(1)	0.25	0	1.2(5)	4*c*
$R_{wp} = 15.97\%$	O(3)	1.03(2)	0.066(1)	−0.065(2)	0.25	1.5(5)	4*d*
$R_p = 11.57\%$	O(4)	1.01(2)	0.383(1)	0.048(3)	0.25	4.1(6)	4*d*

Note. All $KLnTiO_4$ phases crystallize in space group *Pbcm* (#57).

parameters than the rest of the $KLnTiO_4$ series, which is reasonable considering the larger size of the La^{3+} cation. There is a slight increase in the **b** and **c** lattice parameters for Nd through Dy, which could indicate that as the degree of distortion and tilting increases for the smaller lanthanides, the perovskite plane of the unit cell increases in area to accommodate the buckling of the octahedra. This increase in the **b** and **c** lattice parameters as the atomic radius of the lanthanide cation decreases is offset by the decrease in the **a** lattice parameter since the unit-cell volume decreases as the size of the lanthanide cation decreases for all the lanthanides (Table 2).

The $NaLnTiO_4$ phases adopt tetragonal symmetry for the larger lanthanides (Ln = La, Nd), while a transition to orthorhombic symmetry is observed for the smaller lanthanides (Ln = Sm, Eu, Gd, Dy) (17). For the smaller lanthanides, the TiO_6 octahedra become more distorted from ideal tetragonal symmetry to accommodate the smaller Ln^{3+} cations. In contrast, all the $KLnTiO_4$ phases are orthorhombic. For $KLnTiO_4$, the lanthanide radius decreases as the difference between the **b** and **c** lattice parameters also decreases. For the smallest lanthanide, $KDyTiO_4$, there is essentially no orthorhombic distortion, and the symmetry is pseudotetragonal. Apparently, the larger K^+ cation increases the distortion to orthorhombic symmetry for all the lanthanides since it does not fit as well as Na^+ in the rock-salt AO (A = alkali) layer. The buckling of the TiO_6 octahedra is greatest for $KDyTiO_4$, which is necessary to accommodate the smaller Dy^{3+} cation. As a result, the bonding of K^+ with the surrounding oxygen atoms is better optimized, allowing the larger K^+ cation to fit better without distorting to orthorhombic symmetry.

It is worth noting that the hydrothermal synthesis of $KLaTiO_4$ has been previously reported (26), but was not extended to other lanthanides. In addition, $KLaTiO_4$ synthesized hydrothermally has broader diffraction peaks, and the structure is slightly different from the $KLnTiO_4$ phases reported here. Hydrothermal $KLaTiO_4$ was found to be tetragonal with a stacking axis lattice parameter of 13.606 Å (26), while $KLaTiO_4$ synthesized through the two-step

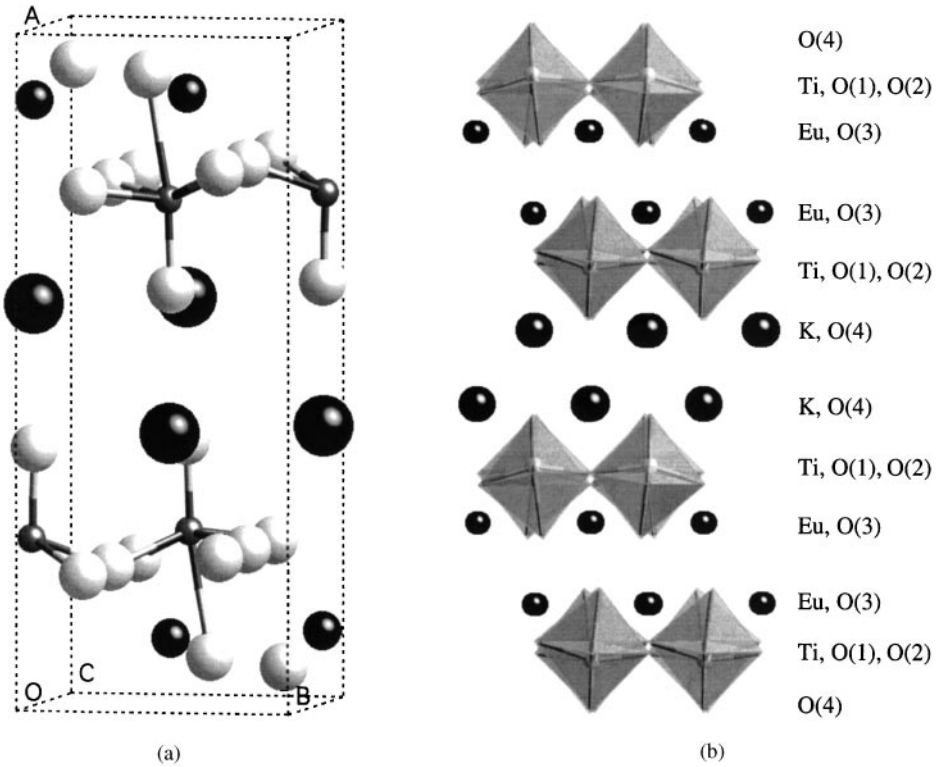

FIG. 4. Crystal structure of $KEuTiO_4$, showing (a) the unit cell in the *Pbcm* space group, and (b) the (011) projection of several unit cells.

ion-exchange route is orthorhombic with a stacking axis lattice parameter of 13.238 Å (Table 2). Both forms of $KLaTiO_4$ hydrate readily in a humidified atmosphere. As noted for other perovskite systems, such as $ZnEu_2Ti_3O_{10}$ (9) and $CaEu_2Ti_2O_8$ (11), the synthetic route can dramatically alter the final structure, even for similar phases of the same stoichiometry. The ion-exchange route to $KLnTiO_4$ preserves the thermodynamically stable $ALnTiO_4$ template, while the hydrothermal synthesis of $KLaTiO_4$ does not involve a template, so it crystallizes differently.

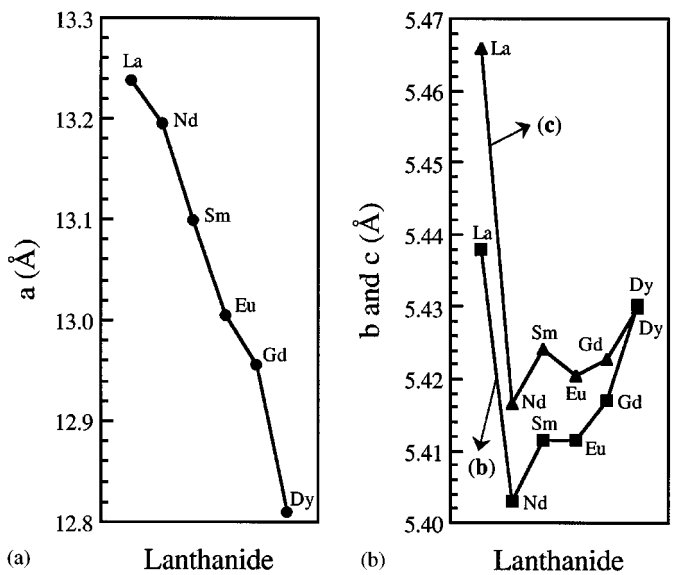

FIG. 5. Plots of (a) the **a**-axis lattice parameter vs lanthanide and (b) the **b**- and **c**-axis lattice parameters *vs* lanthanide for the $KLnTiO_4$ series.

$KLnTiO_4$ Hydrates

When exposed to a humidified atmosphere, all the $KLnTiO_4$ phases readily form hydrates by intercalating water into the ion-exchangeable interlayer gallery. XRD patterns for representative members of the $KLnTiO_4 \cdot xH_2O$ series are shown in Fig. 6. All the phases index to a tetragonal unit cell, with lattice parameters that are expanded along the stacking axis to accommodate the intercalated water. While the parent $KLnTiO_4$ phases are orthorhombic, preliminary evidence suggests that the hydrated phases are tetragonal, which is reasonable considering the significant dependence of the interlayer structure of layered perovskites on the coordination and bonding of the intercalated water (27). Identical hydration behavior occurs for $NaEuTiO_4$, where the stable $NaEuTiO_4 \cdot 0.8H_2O$ hydrated phase appears tetragonal while the anhydrous $NaEuTiO_4$ phase is orthorhombic (28). More detailed structural analyses are required to determine unambiguously

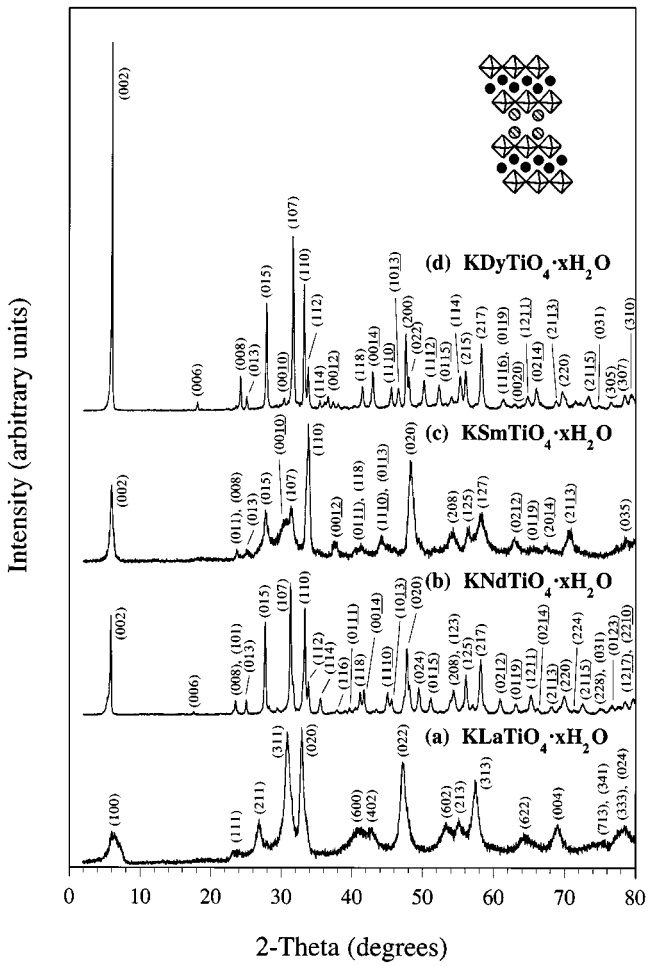

FIG. 6. XRD patterns for (a) $KLaTiO_4 \cdot xH_2O$ [$a = 14.67(9)$, $c = 5.435(7)$], (b) $KNdTiO_4 \cdot xH_2O$ [$a = 3.8028(4)$, $c = 30.295(5)$], (c) $KSmTiO_4 \cdot xH_2O$ [$a = 3.756(6)$, $c = 29.53(4)$], and (d) $KDyTiO_4 \cdot xH_2O$ [$a = 3.8134(3)$, $c = 29.501(5)$]. The inset in (d) shows the structural model for the KLnTiO$_4 \cdot x$H$_2$O (Ln = Nd, Sm, Eu, Gd, Dy) hydrates, which have an eclipsed conformation along the ion-exchangeable interlayer gallery.

whether the KLnTiO$_4 \cdot x$H$_2$O phases are tetragonal or orthorhombic.

The hydrated KLnTiO$_4 \cdot x$H$_2$O (Ln = Nd, Sm, Eu, Gd, Dy) phases adopt an eclipsed rather than a staggered geometry. The shift of the perovskite slabs along the (110) direction (where the **c** axis is the stacking axis) is shown in the inset in Fig. 6. The shift to an eclipsed geometry occurs only along the ion-exchangeable interlayer gallery where the water is intercalated. The interlayer lanthanide layer remains staggered, creating an interesting mixed staggered/eclipsed geometry that is also observed for $NaEuTiO_4 \cdot 0.8H_2O$ (28) and $CaEu_2Ti_2O_8$ (11), which have similar interlayer stacking. Interestingly, $KLaTiO_4 \cdot xH_2O$ appears to retain the staggered geometry of its anhydrous form, and its X-ray diffraction pattern (Fig. 6a) looks almost identical to that of the anhydrous phase (Fig. 2a), except for an increase of 1.43 Å along the stacking axis.

The extent of hydration of the KLnTiO$_4 \cdot x$H$_2$O phases varies, and some of the phases appear to intercalate more water upon extended exposure to a humidified atmosphere. A rough estimate of the extent of hydration was obtained by determining the weight loss upon heating the hydrated phases to 500°C for 12 h. $KLaTiO_4$, $KGdTiO_4$, and $KDyTiO_4$ appear to form trihydrates, while $KSmTiO_4$ and $KNdTiO_4$ intercalate 2.0 and 2.5 waters of hydration per formula unit, respectively. $KEuTiO_4$ does not appear to form a stable dihydrate or trihydrate, but intercalates up to 15 waters of hydration upon extended exposure to a humidified atmosphere (much like the $n = 3$ Ruddlesden–Popper phase $K_2CaNaTa_3O_{10} \cdot xH_2O$ (8e)). The $KDyTiO_4 \cdot xH_2O$ and $KNdTiO_4 \cdot xH_2O$ hydrates are highly crystalline, while the others form more amorphous hydrates. Unfortunately, there is no obvious correlation between structure and degree of hydration or crystallinity. More detailed thermal analysis and comparison to structural data are necessary to elucidate the true structure and hydration level of these phases as well as to determine the correlation between hydration behavior and possible photocatalytic activity.

CONCLUSIONS

In this paper, we have described a two-step ion-exchange approach for preparing KLnTiO$_4$, a series of $n = 1$ Ruddlesden–Popper phases that are inaccessible at high temperatures. By using acid/base chemistry instead of charge density as a driving force for ion exchange, large monovalent cations can be exchanged into a layered perovskite host. Using this approach, it may be possible to design new Ruddlesden–Popper phases that have larger interlayer cations or possibly a solid solution of mixed interlayer cations, which could allow greater control over the interlayer hydration and reactivity of layered perovskites. The KLnTiO$_4$ phases readily hydrate, which may indicate that they could be interesting photocatalysts for splitting water.

ACKNOWLEDGMENTS

This work was supported by the National Science Foundation Grant CHE-0095394. This material is based upon work supported under a National Science Foundation Graduate Fellowship.

REFERENCES

1. F. S. Galasso, "Structure, Properties and Preparation of Perovskite-Type Compounds." Pergamon Press, Oxford, 1969.
2. (a) K. D. Otzschi, K. R. Poeppelmeier, P. A. Salvador, T. O. Mason, H. Zhang, and L. D. Marks, *J. Am. Chem. Soc.* **118,** 8951 (1996). (b) P. A. Salvador, K. B. Greenwod, J. R. Mawdsley, K. R. Poeppelmeier, and T. O. Mason, *Chem. Mater.* **11,** 1760 (1999).

3. Y. Moritomo, A. Asamitsu, H. Kuwahara, and Y. Tokura, *Nature* **380,** 141 (1996).
4. (a) B. Brahmaroutu, G. L. Messing, S. Trolier-McKinstry, and U. Selvaraj, *in* "Proc. 10th IEEE Int. Symp. on Applications of Ferroelectrics, Vol II" (B. M. Kulwicki, A. Amin, and A. Safari, Eds.), pp. 883–886. IEEE, Piscataway, NJ, 1996. (b) M. Seabaugh, S.-H. Hong, and G. L. Messing, *in* "Ceramic Microstructure: Control at the Atomic Level" (A. P. Tomsia and A. Glaeser, Eds.), pp. 303–310. Plenum Press, New York, 1998. (c) T. Takeuchi, T. Tani, and T. Satoh, *Solid State Ionics* **108,** 67 (1998). (d) T. Tani, *J. Kor. Phys. Soc.* **32,** S1217 (1998). (e) J. Horn, S. C. Zhang, U. Selvaraj, G. L. Messing, and S. Trolier-McKinstry, *J. Am. Ceram Soc.* **82,** 921 (1991). (f) P. W. Rehrig, S.-E. Park, S. Trolier-McKinstry, G. L. Messing, B. Jones, and T. R. Shrout, *J. Appl. Phys.* **86,** 1657 (1999).
5. (a) T. Takata, Y. Furumi, K. Shinohara, A. Tanaka, M. Hara, J. N. Kondo, and K. Domen, *Chem. Mater.* **9,** 1063 (1997). (b) H. G. Kim, D. W. Hwang, J. Kim, Y. G. Kim, and J. S. Lee, *Chem. Commun.* 1077 (1999).
6. (a) S. N. Ruddlesden and P. Popper, *Acta Crystallogr.* **10,** 538 (1957); *Acta Crystallogr.* **11,** 54 (1958). (b) S. Uma, A. R. Raju, and J. Gopalakrishnan, *J. Mater. Chem.* **3,** 709 (1993).
7. (a) M. Dion, M. Ganne, and M. Tournoux, *Mater. Res. Bull.* **16,** 1429 (1981). (b) A. J. Jacobson, J. W. Johnson, and J. T. Lewandowski, *Inorg. Chem.* **24,** 3727 (1985). (c) M. M. J. Treacy, S. B. Rice, A. J. Jacobson, and J. T. Lewandowski, *Chem. Mater.* **2,** 279 (1990).
8. (a) J. Gopalakrishnan and V. Bhat, *Inorg. Chem.* **26,** 4301 (1987). (b) B. Dulieu, J. Bullot, J. Wery, M. Richard, and L. Brohan, *Phys. Rev. B* **53,** 10641 (1996). (c) P. J. Ollivier and T. E. Mallouk, *Chem. Mater.* **10,** 2585 (1998). (d) M. Fang, C. H. Kim, and T. E. Mallouk, *Chem. Mater.* **11,** 1519 (1999). (e) R. E. Schaak and T. E. Mallouk, *J. Solid State Chem.* **155,** 46 (2000).
9. R. E. Schaak and T. E. Mallouk, *J. Am. Chem. Soc.* **122,** 2798 (2000).
10. (a) T. A. Kodenkandath, J. N. Lalena, W. L. Zhou, E. E. Carpenter, C. Sangregorio, A. U. Falster, W. B. Simons, Jr., C. J. O'Connor, and J. B. Wiley, *J. Am. Chem. Soc.* **121,** 10743 (1999). (b) J. Gopalakrishnan, T. Sivakumar, K. Ramesha, V. Thangadurai, and G. N. Subbanna, *J. Am. Chem. Soc.* **122,** 6237 (2000). (c) T. A. Kodenkandath, A. S. Kumbhar, W. L. Zhou, and J. B. Wiley, *Inorg. Chem.* **40,** 710 (2001).
11. R. E. Schaak, E. N. Guidry, and T. E. Mallouk, *J. Chem. Soc. Chem. Commun.*, in press.
12. K. Hyeon and S. Byeon, *Chem. Mater.* **11,** 352 (1999).
13. K. Toda, S. Kurita, and Sato, *J. Ceram. Soc. Jpn.* **104,** 140 (1996).
14. (a) J. N. Lalena, B. L. Cushing, A. U. Falster, W. B. Simmons, Jr., C. T. Seip, E. E. Carpenter, C. J. O'Connor, and J. B. Wiley, *Inorg. Chem.* **37,** 4484 (1998). (b) C. H. Mahler, B. L. Cushing, J. N. Lalena, and J. B. Wiley, *Mater. Res. Bull.* **33,** 1581 (1998). (c) B. L. Cushing and J. B. Wiley, *Mater. Res. Bull.* **34,** 271 (1999).
15. R. A. McIntyre, A. U. Falster, S. Li, W. B. Simmons, Jr., C. J. O'Connor, and J. B. Wiley, *J. Am. Chem. Soc.* **120,** 217 (1998).
16. For example, $K_2La_2Ti_3O_{10}$ forms a stable hydrate, $K_2La_2Ti_3O_{10} \cdot 2H_2O$, but $Na_2La_2Ti_3O_{10}$ does not hydrate.
17. (a) G. Blasse, *J. Inorg. Nucl. Chem.* **30,** 656 (1968). (b) K. Toda, Y. Kameo, S. Kurita, and M. Sato, *J. Alloys Compd.* **234,** 19 (1996). (c) S.-H. Byeon and K. Park, *J. Solid State Chem.* **121,** 430 (1996).
18. S.-H. Byeon, J.-J. Yoon, and S.-O. Lee, *J. Solid State Chem.* **127,** 119 (1996).
19. V. Thangadurai, G. N. Subbanna, and J. Gopalakrishnan, *J. Chem. Soc., Chem. Commun.* 1300 (1998).
20. H. M. Rietveld, *J. Appl. Crystallogr.* **2,** 65 (1969).
21. A. C. Larson, and R. B. von Dreele, "Program version: PC-98." Los Alamos National Lab. Rep. No. LA-UR-86-748, 1994.
22. R. E. Schaak, D. Afzal, and T. E. Mallouk, unpublished results.
23. A. J. Jacobson, J. T. Lewandowski, and J. W. Johnson, *Mater. Res. Bull.* **25,** 679 (1990).
24. R. E. Schaak, and T. E. Mallouk, unpublished results.
25. (a) N. S. P. Bhuvanesh and J. Gopalakrishnan, *J. Mater. Chem.* **7,** 2297 (1997). (b) T. A. Kodenkandath and J. B. Wiley, *Mater. Res. Bull.* **35,** 1737 (2000).
26. D. R. Chen, X. L. Jiao, and R. R. Xu, *Mater. Res. Bull.* **34,** 685 (1999).
27. S. H. Byeon and H. J. Nam, *Chem. Mater.* **12,** 1771 (2000).
28. K. Toda, Y. Kameo, S. Kurita, and M. Sato, *Bull. Chem. Soc. Jpn.* **69,** 349 (1996).